Comparative Modeling of Heat and Mass Transfer in Manual and Gas Metal Arc Welding Including Heat Sources and Reacting Forces

Mbonde Noel

Mechanical Engineering Department Mbeya University of Science and Technology, Mbeya, TANZANIA.

noelmbonde@yahoo.com

ABSTRACT

The melting of the wire is a fundamental characteristic of Manual Metal Arc and Gas Metal Arc welding which influences process stability, productivity, and weld bead shape. The present work describes a model developed to calculate Heat and Mass transfer during the welding process including the effects of joule heating, Electron condensation, Cohesive and Magnetic forces. These forces have significant effects on the transient distributions of current density, Heat and mass transfer in Manual Metal Arc and Gas Metal Arc Welding. It has also been proven that physical properties of shielding gases and electrode covers affects some of arc characteristics like metal transfer, wetting behavior, depth of penetration, shape of penetration, travel speed and easy of arc starting. In this paper it has been shown that, proper doping of inert gases with reasonable amounts of active components such as CO_2, NO or O_2 results in better arc stabilization and therefore better heat and mass transfer. The dissociation energy of polyatomic components in gas mixtures enhance the heat input to the base material due to the energy released by recombination. If these results be fully utilized, failure of fabricated equipment in industries, especially SMEs will completely be eliminated. The results were compared to the results obtained from the experiments and various literatures.

Keywords: Modeling, MMAW, GMAW, Joule heating, Electron condensation, Magnetic forces, Cohesive force, Heat and Mass Transfer; Droplet forces.

INTRODUCTION

In GMAW, electric arc-welding processes consist of an electrode and a work piece with opposite polarities. An arc is struck by applying an electric field between two electrodes causing current to flow through the ionized gas column established between them. The heat generated within the arc produces the high temperatures needed to sustain the gas in its ionized state. Thermal energy is transferred to the work piece primarily due to particle fluxes causing it to melt. [1, 2] Subsequent solidification of this molten region forms the weld or actual joint. The temperature of the droplet is due to the contribution of Joule heating and the heat of electron condensation on the surface of the droplet.

The computational domain has an anode region, an arc region and a cathode region. For GMAW, the anode region is the electrode, and the cathode region is the work piece. The differential equations governing the arc, the electrode, and the work piece can be put into a single set [3, 4, 5, and 6]. The differential equations governing the conservation of mass, momentum, and energy based on the continuum formulation are employed in the present study, and the current continuity equation is used to calculate the current density distribution [7, 8, and 9].

ISSN: 2223-9944, e ISSN: 2223-9553

FORCES ACTING ON A MOLTEN DROPLET

In GMAW a combination of forces acts on the droplet and cause it either to hang or fall off the tip. These forces includes Electromagnetic force F_{em} ,Drag force due to flow of shielding gas F_D ,Force of Gravity F_g ,Surface tension force F_γ , Axial magnetic force due to electromagnetic induced pressure F_{am} and Cohesive forces between the particles forming the droplets F_c. The new introduced Cohesive Force F_c is the force that tends to hold the individual molten particles of an electrode together and thus forming a whole spherical arc droplet. This force is the results of unlike charge attraction between molecules of the same material. This force does promote the detachment and is calculated using the formula: $F_c = \sqrt{d_1 d_2 \xi}$, Where d_1 and d_2 are the diameters of the particles in proximity. Combining the derivation of all other known forces (*not shown in this paper*), a new formula for global droplet force is obtained: $F_{Droplet} = F_{em} + F_D + F_g + (-F_\gamma) + F_{am} + F_c =$

$$\frac{\mu_o I^2}{4\pi}\left[\ln\left(\frac{r\sin\theta}{r_w}\right) - \frac{1}{4} - \frac{1}{1-\cos\theta} + \frac{2}{(1-\cos\theta)^2}\ln\left(\frac{2}{1+\cos\theta}\right)\right] + C_D A_p\left(\frac{\rho_{gV_g^2}}{2}\right) + \rho\frac{4}{3}\pi r^3 g$$

$$-2\pi r_w \gamma f + \gamma\left[\frac{1}{r-dR} - \left(\frac{2\pi}{\lambda}\right)^2 dR\right] - \gamma\left[\frac{1}{r+dR} + \left(\frac{2\pi}{\lambda}\right)^2 dR\right] + \sqrt{d_1 d_2 \xi} \quad \ldots\ldots\ldots\ldots\ldots (7)$$

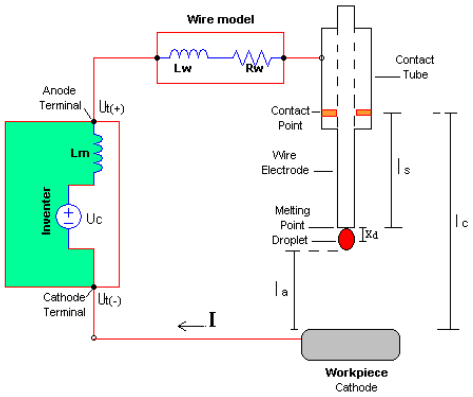

Figure. 1: General welding electrical circuit.

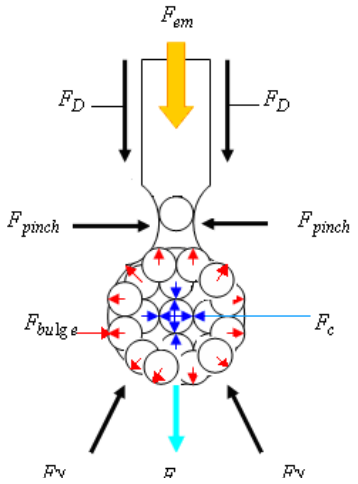

Figure 2: Forces acting on the droplet

ELECT RODE ANALYSIS:

The electrode is modeled as a cylindrical rod subjected to internal and external heating. The various heat sources are due to the following [10]:

Joule heating.

This is because of the current flowing through the electrode. The current is assumed to have a Gaussian distribution along the length of the electrode because of electron flux at the shielding-gas/electrode interface.

ISSN: 2223-9944, e ISSN: 2223-9553

Electron condensation.

This occurs due to ionization of the shielding gas. The electrons released in the gas as a result try to enter the electrode through its surface, and in the process, release energy in the form of heat. Some part of this energy may be lost to the surroundings. Assuming that conduction will be the dominant mode of heat transfer inside the electrode, we model the electrode for axisymmetric conduction heat transfer with the following governing equation:

$$\rho V_w \frac{\partial H}{\partial x} = \frac{\partial}{\partial x}\left(\frac{k}{c_p}\frac{\partial H}{\partial x}\right) + \frac{1}{r}\frac{\partial}{\partial r}\left(\frac{kr}{c_p}\frac{\partial H}{\partial r}\right) + q''' \quad \text{.............................. (1)}$$

where V_w is the wire feed rate, H is the enthalpy, and q''' represents the volumetric heat generation due to Joule heating. For any axial distance *x*, q''' can be expressed as [10],

$$q''' = \left\{\frac{\alpha I}{\sqrt{2\pi r_w^{3}\sigma}}\exp\left[-\frac{(L-x)^2}{2\sigma^2}\right]\right\}^2 \rho_e \quad \text{..(2)}$$

where α is the fraction of heat input due to electron condensation, σ is the distribution parameter for the electrons, r_w is the radius of the electrode wire, L is the total length of the electrode, and I is the current. It is assumed here that q''' is uniform across the cross section of the electrode and varies only along its length.

Boundary conditions (electrode)

The governing equation (1) is solved using the following boundary conditions: At *x*=0 (entry of electrode at the nozzle): $T = T_{\text{int}}$ …..…………………………………….… (3)

where T_{int} is the ambient temperature. At $r = r_w$ (side wall):

$$q_s'' = \left\{\frac{\alpha I V_c}{\pi r_w}\frac{1}{\sigma\sqrt{2\pi}}\exp\left[-\frac{(L-x)^2}{2\sigma^2}\right]\right\} \quad \text{…. (4)}$$

where q_s'' represents the Gaussian heat flux distribution due to electron condensation, and V_c is the apparent voltage drop at the electrode surface [8]. V_c is a constant for any given material (e.g., $V_c = 6V$ for steel).

At $r = 0$ (centerline of the electrode): $\frac{\partial T}{\partial r} = 0$ ………………… (5)

The temperature field in the cylindrical domain is calculated using a fixed grid finite-volume method for a given current, wire feed rate, and radius of the electrode. A pseudo-transient mode is used, and calculations are performed until a steady state is reached. The temperature is expected to depend primarily on the fraction α of heat input due to electron condensation, which depends on the shielding gas-metal combination (argon-steel in this case). The output of this module is the droplet temperature, which is the same as the electrode tip temperature. The specific enthalpy of the molten droplet is calculated as: $h_{drop} = \Delta H + c_p \Delta T$ ….…… (6)

where ΔH is the latent heat required to melt the electrode, and ΔT is the difference between the droplet temperature and the electrode entry temperature (i.e., ambient temperature). The rate of energy input into the work piece due to falling droplets is given by:

$$\dot{H}_{drop} = \dot{m}_{drop} h_{drop} \quad \ldots\ldots\ldots\ldots (7)$$

where $\dot{m}_{drop}$ is the mass flow rate of the molten droplets, and can be calculated as:

$$\dot{m}_{drop} = \rho\pi r_w^2 V_w \quad \ldots\ldots (8)$$

THE WELD POOL ANALYSIS:

The schematic diagram (Figure 4) shows the various forms of heat input to and losses from the work piece. The total energy input to the system is VI. Part of this energy is used to heat and melt the electrode, which finally enters the weld pool in the form of droplet enthalpy, H_{drop}. The balance energy supplied is dissipated as arc heat, part of which enters the work piece with an efficiency factor, η. The above forms of heat input cause the heating of the work piece and formation of the weld pool. Some heat is lost due to convection and radiation from the surface. Once these are specified, the remaining task is to solve the governing equations for heat transfer and fluid flow, with proper initial and boundary conditions.

The Governing Equations

The heat transfer and fluid flow in moving arc welding is a three-dimensional process. The process in the entire work piece is modeled using a single-domain enthalpy-porosity technique [14] with appropriate source terms in the momentum conservation equations, which allow a smooth transition in the velocities ranging from zero in the solid region to a finite value in the liquid domain. In this method, the solid-liquid interface comes out as part of the solution, and hence it is not required to track it separately. For the sake of convenience of study, the governing transport equations are transformed into a coordinate system attached to the arc, which travels at a constant speed, U_{scan}. Although the fully developed weld pool in the moving coordinate system will eventually reach a quasi-steady state, the transient terms in the momentum and energy equations are preserved in our formulation. This is done in order to capture the transient evolutionary development of the molten pool, which plays a significant role in determining its final shape and size. The three-dimensional governing transport equations for the entire domain are given as follows.

Continuity:

$$\frac{\partial}{\partial x}(\rho u)+\frac{\partial}{\partial y}(\rho v)+\frac{\partial}{\partial z}(\rho w)=0 \quad \ldots\ldots\ldots\ldots\ldots\ldots\ldots\ldots\ldots\ldots\ldots\ldots (9)$$

***x*- Momentum**:

$$\frac{\partial}{\partial t}(\rho u)+\frac{\partial}{\partial x}(\rho uu)+\frac{\partial}{\partial y}(\rho uv)+\frac{\partial}{\partial z}(\rho uw)=-\frac{\partial p}{\partial x}+\frac{\partial}{\partial x}\left(\mu\frac{\partial u}{\partial x}\right)+\frac{\partial}{\partial y}\left(\mu\frac{\partial u}{\partial y}\right)+\frac{\partial}{\partial z}\left(\mu\frac{\partial u}{\partial z}\right)+S_x+\frac{\partial}{\partial x}(\rho U_{scan}u) \ldots. (10)$$

y- Momentum

$$\frac{\partial}{\partial t}(\rho v)+\frac{\partial}{\partial x}(\rho uv)+\frac{\partial}{\partial y}(\rho vv)+\frac{\partial}{\partial z}(\rho vw)=-\frac{\partial p}{\partial y}+\frac{\partial}{\partial x}\left(\mu\frac{\partial v}{\partial x}\right)+\frac{\partial}{\partial y}\left(\mu\frac{\partial v}{\partial y}\right)+\frac{\partial}{\partial z}\left(\mu\frac{\partial v}{\partial z}\right)+S_y+\frac{\partial}{\partial x}(\rho U_{scan}v) \ldots\ldots 11)$$

ISSN: 2223-9944, e ISSN: 2223-9553

z- Momentum:

$$\frac{\partial}{\partial t}(\rho w)+\frac{\partial}{\partial x}(\rho uw)+\frac{\partial}{\partial y}(\rho vw)+\frac{\partial}{\partial z}(\rho ww)=-\frac{\partial p}{\partial z}+\frac{\partial}{\partial x}\left(\mu\frac{\partial w}{\partial x}\right)+\frac{\partial}{\partial y}\left(\mu\frac{\partial w}{\partial y}\right)+\frac{\partial}{\partial z}\left(\mu\frac{\partial w}{\partial z}\right)+S_z+\frac{\partial}{\partial x}(\rho U_{scan} w)\cdots\cdots 12)$$

In the present enthalpy-porosity formulation, the source terms in the above momentum equations take the following form:

$$S_x=-\left[\frac{C(1-\varepsilon)^2}{\varepsilon^3+b}\right]u+(J\times B)_x \ldots\ldots(13)$$

$$S_y=-\left[\frac{C(1-\varepsilon)^2}{\varepsilon^3+b}\right]v+(J\times B)_y+\rho g\beta(T-T_m)\ldots\ldots(14)$$

$$S_z=-\left[\frac{C(1-\varepsilon)^2}{\varepsilon^3+b}\right]w+(J\times B)_z \ldots\ldots(15)$$

where the first terms in each of Eqs. (13)-(15) represent the porous medium model of the mushy region at the solid-liquid interface, and the $J\times B$ terms are the Lorentz force components in the respective directions. The *y* momentum source term also includes the buoyancy force due to thermal expansion. The terms containing U_{scan} are additional source terms appearing as a result of the coordinate transformation [16]. The liquid volume fraction ε has a value of 0 in the solid phase, 1 in the liquid phase, and between 0 and 1 in the mushy region. *C*, the morphological constant, is a number that is made sufficiently large (say, 10^8) such that the velocities in the momentum equations are driven to 0 in the solid region. In the liquid phase, however, $\varepsilon=1$, and therefore *C* has no role to play. The constant b in the porosity source term is a small number (say, 10^{-3}) used to prevent any division by 0 in the solid region.

Energy Conservation:

$$\frac{\partial}{\partial t}(\rho c_p T)+\frac{\partial}{\partial x}(\rho c_p uT)+\frac{\partial}{\partial y}(\rho c_p vT)+\frac{\partial}{\partial z}(\rho c_p wT)=\frac{\partial}{\partial x}\left(k\frac{\partial T}{\partial x}\right)+\frac{\partial}{\partial y}\left(k\frac{\partial T}{\partial y}\right)+\frac{\partial}{\partial z}\left(k\frac{\partial T}{\partial z}\right)-\frac{\partial}{\partial t}(\rho\Delta H)+\frac{\partial}{\partial x}(\rho c_p U_{scan} T)$$

$$+\frac{\partial}{\partial x}(\rho U_{scan}\Delta H)+S_{drop} \ldots\ldots (16)$$

In Eq. (16), ΔH represents the enthalpy change due to phase change (latent heat), the two terms containing U_{scan} appear as a result of the coordinate transformation, and S_{drop} is an energy source term accounting for a volumetric heat addition due to falling droplets from the melting electrode. The energy transfer by the falling metal droplets is partly responsible for the ``finger'' penetration in the GMAW process. This energy is assumed to be distributed uniformly in an imaginary cylindrical cavity as described in [8, 15]. This method of distributing droplet heat energy takes into consideration the momentum and thermal energy of the falling droplets.

Boundary Conditions (Work Piece)

Since the present formulation is based on a single domain (for both liquid and solid) method, the boundary conditions can be specified for the entire work piece domain. In this method, the solid-liquid interface comes out as part of the solution, and hence the interface does not have to be

tracked separately, and no separate condition needs to be imposed there. The following are the boundary conditions for the primitive variables (*u*; *v*; *w*; and *T)* with reference to the work piece.

Top surface: $-k\frac{\partial T}{\partial y} = -q_{arc}^{"} + h(T - T_{\alpha}) + \sigma_r \varepsilon_r \left\{T^4 - T_{\alpha}^4\right\}$ ..... (17)

where $q_{arc}^{"}$ is the net heat flux from the arc distributed in a Gaussian manner (with a radius r_q) on the surface of the weld pool and is expressed as : $q_{arc}^{"} = \frac{(VI - h_{drop}\dot{m}_{drop}}{\pi r_q^2}\exp\left[-\frac{r^2}{r_q^2}\right]$ .....18)

Because of large temperature gradients on the pool surface, the surface tension (which is temperature dependent) varies greatly. Liquid is pulled in the direction of increasing surface tension. This surface tension force is balanced by the viscous shear forces. Assuming a flat surface, we give the velocity conditions by:

$$\mu\frac{\partial u}{\partial y} = \sigma_s\frac{\partial T}{\partial x}; \qquad \mu\frac{\partial w}{\partial y} = \sigma_s\frac{\partial T}{\partial z} \qquad and \qquad v = 0 \text{ ..... (19)}$$

Sides: Convective heat loss and solid walls: $h(T - T_{\alpha}) = -k\frac{\partial T}{\partial \eta}$ and $u = v = w = 0$ ..... (20)

Bottom: Insulated and solid wall condition: $k\frac{\partial T}{\partial y} = 0$ and $u = v = w = 0$ ..... (21)

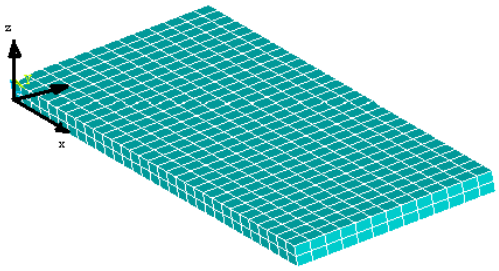

Figure3: Three-dimensional finite element model for thermo-mechanical analysis.

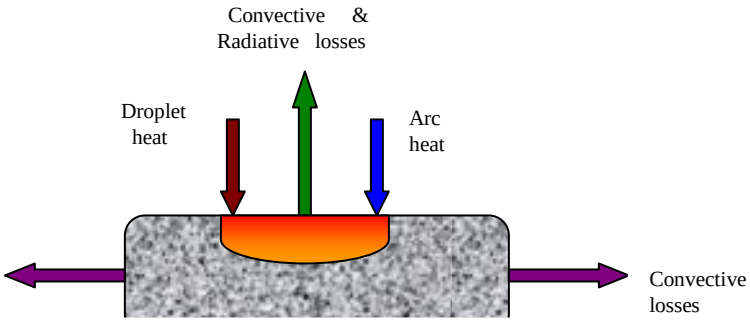

Fig.4:Variaous forms of heat inputs and heat losses on the work piece

Experimental Procedure

Five shielding gas mixtures [Argon + 2%CO_2, 100%argon, Argon + 2%CO_2, , Argon +5%CO_2 and Argon + 15%CO_2 on GMAW process were used for the purpose of:

(i) Analyzing **transfer modes** , **Heat and mass transfer** in different shielding gas compositions,

(ii) Analyzing Weld bead dimensions (**Width, Height, and Depth of penetration)** on the base metal caused by the above mentioned shielding gas mixtures.

ISSN: 2223-9944, e ISSN: 2223-9553

Several Bead-on-plate welding tests were made on steel plates EN8 using electrode wire (AWS ER 70S-6) with a diameter of 1.2 mm. This is a very common consumable, widely used in industries for structural works.

Table 1: Base metal composition:

C%	*S%*	*Cu%*	*Al%*	*Ni%*	*Co%*	*W%*	*Cr%*	*Si%*	*Mn%*	*content*	*P%*
0.24	0.001	0.04	0.001	0.11	0.02	0.05	0.03	0.16	0.69	B/Metal	0.02

RESULTS AND DISCUSSION

Metal Transfer Modes

During the tests, the mean values of current and voltage, corresponding to each type of transfer, were registered and transfer mode maps for each mixture were developed-Figure (6a-6d). The parameters used during the test are illustrated in Table 2. The determination of metal transfer modes and definition of the mode boundaries were made with the help of data analysis, visual inspection and arc sound. In this analysis three main properties of base metal and gas mixtures-Ionization potential, disassociation energy and thermal dependent properties were considered as factors having potential influence on heat transfer, metal transfer modes and weld bead dimensions Figures 9(a)-9(d). The analysis done with **100% Argon:** (fig. 6(a) & 6(b)), the necessary voltages to obtain a stable metal transfer with pure argon gas lies between 22V and 25 V, but becomes more stable in higher amperages than in lower ones. This indicates that Argon requires higher voltage to arc, due to its low value of ionization potential and lower thermal conductivity and therefore a poor conductor of heat compared to other shielding gases. The analysis of arc transfer mode map done with different combinations of **Argon** with **Carbon dioxide**, revealed that, the necessary voltages to obtain a stable metal transfer increases as the amount of CO_2 in the mixture increases(fig.6(c) & 6(d)). This indicates that the arc stability decreases with the increase of carbon dioxide content in the mixture. This fact is related to the higher thermal conductivity of CO_2, which gives rise to more heat losses by conduction and thus the necessity to use higher voltage, for the same current intensity to initiate and stabilize the arc as compared to other binary gas mixture like (98%Argon + 2%O_2).

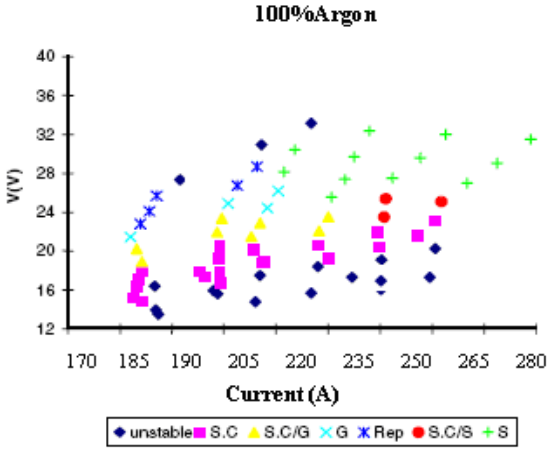

Figure 6(d): Droplet transfer mode map for Argon +5%Carbon.

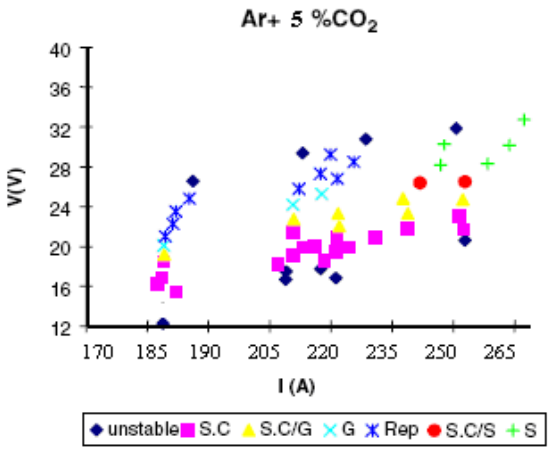

Figure 6(a): Transfer mode map for 100%Argon 95% shielding gas.

ISSN: 2223-9944, e ISSN: 2223-9553

Analysis on the effects of welding parameters on bead dimensions (fig.7 (a) & 7(b), 9(a) – 9(d) and on heat inputs (HI) figure (8) were also made based on data obtained during experiments. Different values of Heat Input and bead dimensions were obtained for different shielding gas composition. Processing the instant values of the arc voltage and current intensity, the mean values were computed for any particular period and used for computation of Heat Inputs (HI). When analyzing the same procedure, important differences were noticed when comparing the HI values for different shielding gas compositions. The HI values are graphically presented in Figure 8. In this study, a 200A current is applied to the electrode from 0 s to 1 s. A complete sequence of electrode melting; droplet formation, detachment, transfer, and impingement onto the work piece; and weld-pool dynamics is calculated. However, in the following paragraphs, results will be presented for the first three droplets' formation, detachment, transfer, and impingement onto the work piece, and weld-pool development; for the weld-pool dynamics after the impingement of the last droplet; and for the solidification process of the electrode and weld pool after the current is turned off. The corresponding temperature distributions in the metal and temperature distributions in both the arc plasma and the metal of these cases are shown in Fig.8

The metal transfer mode of a 1.2-mm diameter mild-steel electrode is globular transfer under a 220-A current. The shape of the droplet shown in Fig.8 is round and is in agreement with the experimental results.

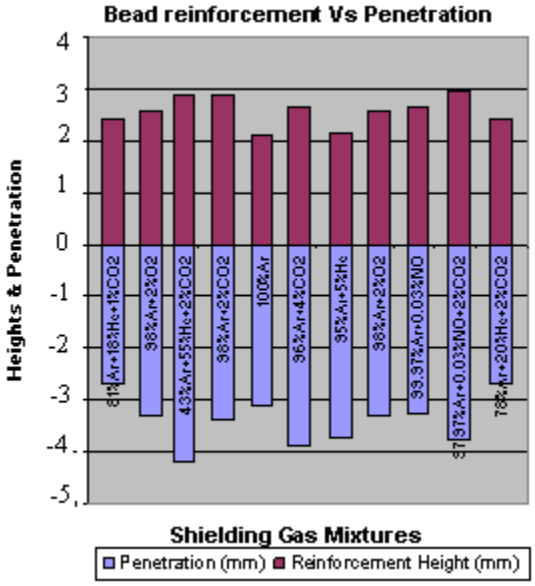

Figure 7a: Dependence of Bead reinforcement and Penetration on shielding gas mixtures.

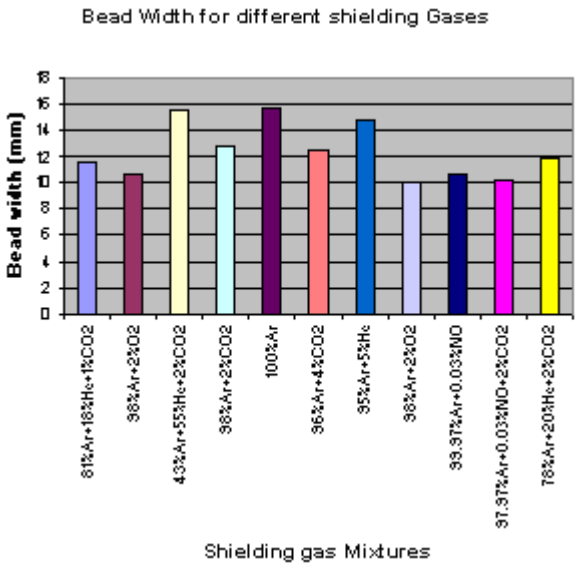

Figure 7(b) Effects of shielding gas mixtures on Weld bead width.

The temperature within the droplet is determined by the concentrated heating at the anode surface and the flow pattern within the droplet. The highest temperature found at the droplet surface is 2936 K, which is in agreement with the experimental data of [10]. The fluid flow pattern within the droplet is caused by a balance of forces acting on the droplet, which includes electromagnetic force, surface tension force, gravity, arc pressure, and plasma shear stress as shown in fig.(2). The detached droplet is accelerated by the plasma arc and gravity. The fluid flow in the detached droplet helps to mix the cold liquid in the droplet center with the hot liquid at the surface. Thus, a more uniform temperature distribution appears in the detached droplet

ISSN: 2223-9944, e ISSN: 2223-9553

than in the droplet hanging at the electrode tip. The detached droplet is continually heated by the surrounding high temperature plasma arc when it is accelerated toward the work piece. Before the droplet impacts the work

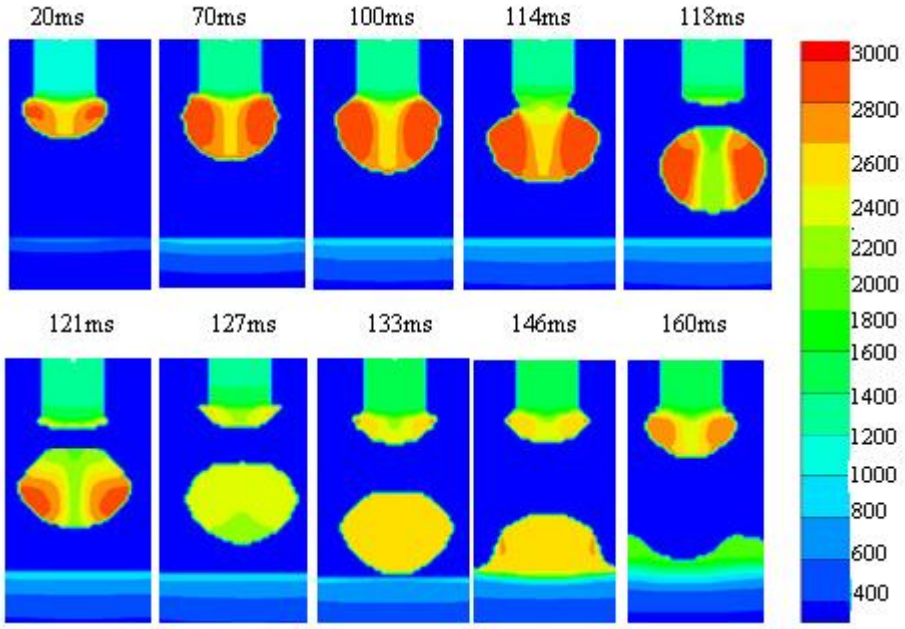

Figure (8): Temperature and mass distribution at different instants to show the effects of the detached droplets and the Deformed weld pool on the arc plasma distribution

Table 2: Numerical results of a typical electrode analysis

Current(A)	*Wire feed speed(mm/s)*	*Wire radius (mm)*	*Wire length (mm)*	*Drop temperature(C)*	*Drop mass rate (kg/s)*
210	138	0.6	25.4	2400	0.001214

Piece, the work piece has also been warmed by the arc plasma, but the surface temperature of the work piece is still low. Some work piece metal is melted by the superheated thermal energy contained by the droplet and mixes with the droplet. Thus, the mass, momentum, and thermal energy carried by the droplet mix and merge into the work piece. A weld pool begins to form. The weld pool temperature continues to drop as it spreads outward and loses heat to the cold base metal by conduction. Due to the heat loss to the solid metal by conduction and to the surroundings by radiation and convection, the sizes of the molten droplet and the weld pool become smaller. As the heat loss occurs mainly through conduction to the solid metal, the liquid metal adjacent to the solid and liquid interface solidifies first. The last liquid zone in the electrode is in the tip of the electrode and the last liquid zone in the weld pool is on the top of the weld pool.

ISSN: 2223-9944, e ISSN: 2223-9553

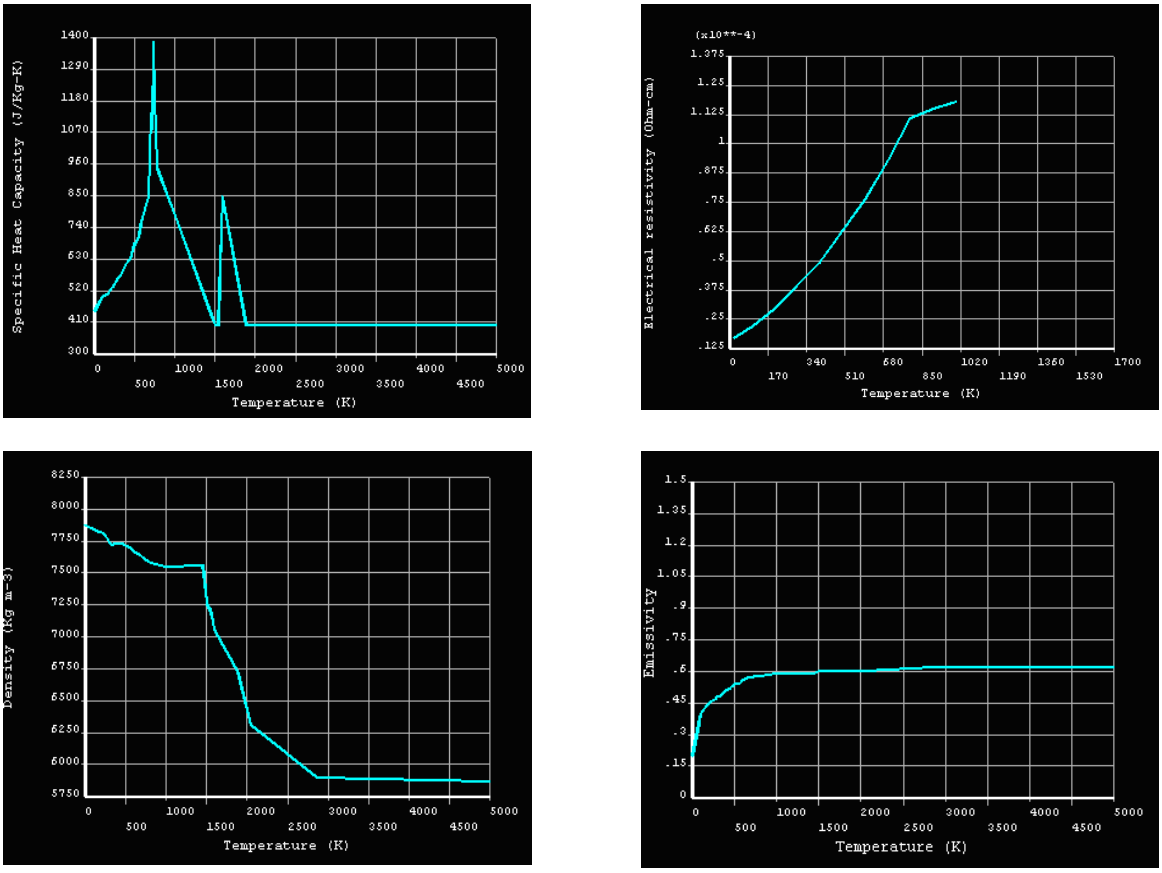

Figure (9 a-d): Dependence of heat transfer on Physical properties of weld metal (N8)

CONCLUSIONS

This special paper presents experimental data on the influence of process parameters and shielding gas composition on droplet formation, transfer modes, Heat transfer and Bead dimensions in gas metal arc welding (GMAW) for each shielding gas composition studied. The data summarizes the differences in GMAW metal transfer modes and their relation to bead dimensions for different gas mixtures. From these results, the following has been concluded:

- The droplet transfer and the deformed weld pool surface have significant effects on the transient distributions of current density, arc temperature and arc pressure.
- Metal transfer is influenced by a number of physical variables, including temperature, velocity, current density, electric potential, magnetic field, electromagnetic force, cohesive forces and pressure. This is caused by the concentrated heating on the anode spot and the convection pattern within the droplet.
- Under the continuous arc heating, the temperature of the droplet surface will reach the boiling point and the metal will start to vaporize.
- When a droplet is detached, the thin liquid bridge connecting the droplet and the wire tip may also break and evolve to one or more tiny droplets. These droplets are known as satellite drops

ISSN: 2223-9944, e ISSN: 2223-9553

- The taper formation at higher welding current is closely related to the heat input on the un-melted portion of the welding wire; the globular–spray transition is mainly due to the increased current and electromagnetic pinch force, and the taper formation influences this transition by decelerating the transfer process;
- Since the welding wire is melted by resistive heating and anode reactions, and, to some extent, also by arc heating, the wire surface directly exposed to the arc tends to melt faster than the interior metal.

ISSN: 2223-9944, e ISSN: 2223-9553

REFERENCES

[1]. Allum, C. J., & Quintino, L. (1985).Control of fusion characteristics in pulsed current MIG welding–Part 2. *Metal Construction* 17 5 pp. 314R–317R.

[2]. Brent et al.,(1988). Enthalpy-Porosity Technique for Modeling Convection-Dif usion Phase Change: Application to the Melting of a Pure Metal, *Numerical Heat Transfer*, *13*, pp.297± 318.

[3]. Eagar, T. W., & Kim, S-Y. (1993).Analysis of metal transfer in gas metal arc welding. *Weld J 72*(6):269–78.

[4]. Experimental investigation of the forces acting on a drop of weld metal. Weld J 1983; 62(4):109s–16s. European Directive 86/642/CEE.

[5]. hu et al., (2004). Signature analysis for quality monitoring In Short-circuit GMAW. *Weld J 83(*12):336S–343S.

[6]. J.J. Hunter et al.,(1988). On-line Control of the Arc Welding Process, Proc. 2nd Int. Conf. on Computer Technology in Welding, Cambridge, UK, pp. 37-1–37-12.

[7]. Kannatey- Asibu, E., & Rhee, S. (1992). Observation of metal transfer during gas metal arc welding. *Weld J 71*(10):381–6.

[8]. Lancaster, J. F. (1986).The physics of welding. International Institute of Welding, Pergamon Press.

[9]. Larson, L. J. (1942).Metal transfer in the metallic arc. *Weld J 63*(2):107–12.[10] Waszink JH, Graat LHJ.

[10]. Mbonde Noel, Graeme Oliver, (1996). Analysis and modelling of arc droplet formation in gas metal arc welding (gmaw); Thesis 2008 Cape Peninsula University of Technology.

[11]. N. Christensen et al.(1995, Distribution of temperatures in arc welding, *British Weld. J.* 2, 54–75.

[12]. Norrish, J., &Richardson I. F. (1988). Metal transfer mechanisms. *Weld Metal Fabr. 56(*1):17– 22.

[13]. Pires, I.(1996). Analysis of the influence of shielding gas mixtures on features of MIG/MAG, MSc thesis, Lisbon Technical University.

[14]. Quinn et al., (2005). Coupled arc and droplet model of GMAW source. *Scince and technology Weld Join 10*(1):113–9.

[15]. Smartt et al., **(**1986). Gas metal arc welding process sensing and control, Advances in Welding Science and Technology, Proc. Int. Conf. on trends in welding research, Gatlinburg, Tennessee, USA, pp. 461–465.

[16]. Tekriwal et al., (1987). Finite element modelling of heat transfer for gas metal arc welding. *Metal Construction* 19 7 pp. 599R–606R.

[17]. Terasaki, H., & Simpson, S. W. (2005). Modelling of the GMAW system in free flight and short circuiting transfer. *Sci Technol Weld Join 10*(1):120–124.

ISSN: 2223-9944, e ISSN: 2223-9553